



# Fast neutron induced gamma rays from (n,n'), (n,p) and (n, $\alpha$ ) reactions on CaCO<sub>3</sub>

Niklas Ophoven<sup>1,2</sup> · Zeljko Ilic<sup>1,3</sup> · Eric Mauerhofer<sup>1</sup> · Tsitohaina H. Randriamalala<sup>1</sup> · Egor Vezhlev<sup>1</sup> · Christian Stiegchorst<sup>4</sup> · Zsolt Révay<sup>4</sup> · Thomas Brückel<sup>1,3</sup> · Jan Jolie<sup>2</sup> · Erik Strub<sup>2</sup>

Received: 30 July 2022 / Accepted: 28 September 2022 / Published online: 2 November 2022  
© The Author(s) 2022

## Abstract

Emission of prompt gamma rays following (n,n'), (n,p) and (n, $\alpha$ ) reactions induced by irradiation of a calcium carbonate (CaCO<sub>3</sub>) sample with a beam of fission neutrons was investigated with a modified version of the FaNGaS (Fast Neutron-induced Gamma-ray Spectrometry) instrument operated at the Heinz Maier-Leibnitz Zentrum (MLZ) in Garching. The neutron spectrum has an average energy of 2.30 MeV and at sample position the fast neutron flux was  $(1.13 \pm 0.04) \times 10^8 \text{ cm}^{-2} \text{ s}^{-1}$ . The measurement was performed at an angle of 90° between neutron beam and detector. In total, we claim the identification of 38 prompt gamma lines, from which we have assigned 12 to the (n,n') reaction in calcium (7 for <sup>40</sup>Ca, 1 for <sup>42</sup>Ca and 4 for <sup>44</sup>Ca), 1 to the <sup>12</sup>C(n,n')<sup>12</sup>C reaction, and 2 to the (n,n') reaction in oxygen (1 for <sup>16</sup>O and 1 for <sup>18</sup>O). The other observed gamma lines are attributed to the <sup>40</sup>Ca(n,p)<sup>40</sup>K reaction (20 lines) and to the <sup>40</sup>Ca(n, $\alpha$ )<sup>37</sup>Ar reaction (3 lines). Relative intensities and fast neutron spectrum averaged partial cross sections of the gamma lines are presented and compared with available literature data. Our results were found to be in good agreement with available literature data but also improved and complemented it, as we have pointed out possible errors and identified new lines. Additionally, for a counting time of 12 h the detection limits of calcium, carbon and oxygen were determined as 5, 13 and 64 mg, respectively.

**Keywords** Inelastic scattering · Calcium · Carbon · Oxygen · Cross section · Gamma ray

## Introduction

The feasibility to perform accurate chemical elemental analysis using prompt gamma rays induced by fast neutrons was demonstrated in various works in the past [1–5], worth mentioning our efforts with the instrument FaNGaS (Fast Neutron-induced Gamma-ray Spectrometry) [6–10], which was installed at the Heinz Maier-Leibnitz Zentrum (MLZ) in 2014 and since then continuously optimized to improve the

peak-to-background ratio, i.e. counting statistics. The fast neutrons are produced by a highly-enriched uranium (93% <sup>235</sup>U) converter plate immersed into the moderator of the FRM II (Forschungsreaktor München II). The neutron beam is extracted at the beamtube SR10 (Strahlrohr 10) through a set of filters and collimators into the experimental room of the MEDAPP (Medical Application) facility [11]. The gamma radiation, induced by the interaction of the fast neutron beam with the sample, is detected by a well-shielded high-purity germanium (HPGe) detector that is mounted on a heavy iron carriage and arranged perpendicular with respect to the neutron beam axis. Besides numerical and experimental optimization studies aiming to reduce the beam background and to reach lower detection limits, another major purpose of FaNGaS is to build up a comprehensive data catalogue of (n,n' $\gamma$ ) reactions using state-of-the-art of gamma-ray spectrometry. These data are intended to meet the increasing demand for reliable knowledge on (n,n' $\gamma$ ) neutron inelastic scattering reactions observed in the industrial and scientific community of nuclear science and technology [12–14]. The data shall cover every naturally abundant

✉ Niklas Ophoven  
n.ophoven@fz-juelich.de

<sup>1</sup> Jülich Centre for Neutron Science, Forschungszentrum Jülich GmbH, 52425 Jülich, Germany

<sup>2</sup> Mathematisch-Naturwissenschaftliche Fakultät, Universität zu Köln, 50923 Cologne, Germany

<sup>3</sup> Lehrstuhl Für Experimentalphysik IVc, RWTH Aachen University, 52056 Aachen, Germany

<sup>4</sup> Heinz-Maier-Leibnitz Zentrum (MLZ), Technische Universität München, Lichtenbergstraße 1, 85748 Garching, Germany

element of the periodic system and comprise information on relative intensities and isotopic partial gamma-ray production cross sections measured at an angle of  $90^\circ$  between neutron beam and spectrometer. Recently, a relational database of inelastic neutron scattering ( $n, n'\gamma$ ) data was developed [15] from the only available database in this field: the “Atlas of Gamma-rays from the Inelastic Scattering of Reactor Fast Neutrons”, published by Demidov et al. in 1978 [16]. This “Demidov Atlas”, however, to our knowledge has never been validated yet. Furthermore, a lack of relevant information about the data processing is observed at some points, concerning the procedure for the correction of capture interferences for example. This circumstance impedes an accurate understanding and interpretation of available data. In our previous works [9, 10], we were always able to point out the need for a meticulous reevaluation and to provide enhanced and also additional nuclear data.

Within this work, we present the results of the measurement of prompt gamma rays produced by ( $n, n'$ )-inelastic scattering and ( $n, p$ )- and ( $n, \alpha$ )-capture reactions of fast neutrons on calcium, carbon and oxygen. The measurement was performed with a new version of the FaNGaS instrument comprising a renewed shielding of the spectrometer as well as an upgraded multi-leaf collimator (MLC) of the MEDAPP facility [17]. The fast neutron flux at the sample position was again determined by irradiating the iron foil previously investigated with the former version of the FaNGaS instrument [9]. Relative gamma-ray intensities and fast neutron spectrum averaged partial gamma-ray production cross sections are presented including comparisons with available literature data. Additionally, we present elemental detection limits for calcium, carbon and oxygen.

## Modifications of the FaNGaS instrument

Two major modifications of the FaNGaS instrument were performed. The first one concerns the shielding of the HPGe detector to decrease the beam background, and the second one the collimation of the fast neutron beam due to an upgrade of the MEDAPP facility. In the original version of the FaNGaS spectrometer, the detector was shielded against neutron and gamma ray background with three layers made of 30 cm thick polyethylene (PE, outer layer), 1 cm thick boron carbide ( $B_4C$ , intermediate layer) and 15 cm thick lead with 4% antimony (inner layer) [7]. The lead-antimony bricks were mounted into a 1 mm thick carrier frame made of steel. In a second version shown in [9], the front shielding made of a 30 cm thick PE layer was replaced by a layer of borated PE with 20 wt%  $B_2O_3$  (BPE) of same thickness in order to increase the absorption of thermal neutrons. The origin of

gamma lines attributed to the beam background observed in that spectrum is discussed in [7, 9]. For further reduction of the beam background and also to facilitate the access to the electromechanically cooled HPGe detector the shielding was upgraded. To avoid the production of the long-lived radionuclide  $^{124}Sb$  ( $T_{1/2} = 60.3$  d), the lead-antimony bricks were replaced by blocks of lead-copper ( $Pb_{99.94}Cu$ , standardized nomenclature according to DIN 17640–1 [18]), keeping the total thickness to 15 cm. The steel frame as well as the intermediate layer of boron carbide was removed. The 30 cm thick PE outer layer was replaced by a BPE layer of same thickness. Compared to the previous version [9], the BPE layer covers the full front area of the spectrometer. Additionally, two BPE plates with a thickness of 3 cm can be fixed on both sides of the shielding. For gamma-ray collimation, the previous cylindrical lead collimator was reduced to 10 cm in length and placed as close as possible to the detector. The rest 20 cm in the cylindrical aperture (diameter: 10 cm) of the front shielding were filled with a BPE collimator of same dimensions (inner diameter: 6 cm, wall thickness: 2 cm, length: 20 cm). The spectrometer setup at the experimental position is shown in Fig. 1. The rear part of the shielding is composed of two doors made of BPE and two movable lead stones to access to the detector (see Fig. 1).

In addition, the MEDAPP facility was provided with a new MLC, mounted into the biological-shield wall separating the irradiation room and the filter bench bunker [17]. The leaves consist in the beam direction of a sequence of Fe, BPE (20 wt% B), Fe with BPE inlays, Al and BPE. They are 62 cm in length with a thickness varying between 1.15 and 1.75 cm. For comparison, the leaves of the former MLC were 50 cm long and 1.5 cm wide, and made of a sequence of Fe, PE and Pb (in the beam direction) [11]. The collimator/filters set-up installed in the filter bench bunker [9] is still used for pre-collimation of the fast neutron beam. The aperture of the new MLC is set to  $A_{new} = 5.8 \times 5.8$  cm<sup>2</sup>, almost identical to this set with the former MLC,  $A_{old} = 6 \times 6$  cm<sup>2</sup>. As shown in Fig. 1, the new MLC protrudes around 30 cm from the biological-shield wall. For this reason the spectrometer is shifted 43 cm away from the biological-shield wall and the distance between sample-irradiation position and fast neutron source ( $^{235}U$  converter plate in reactor pool) increases from  $h_{old} = 548$  cm to  $h_{new} = 591$  cm. The distance between the sample and the HPGe detector is kept unchanged to 67 cm. Compared to the former irradiation geometry, a reduction of the fast neutron flux at sample position is expected due to the increase of the distance between sample and neutron source.

The fast neutron flux for the new irradiation geometry  $\Phi_{new}$  can be estimated from the fast neutron flux measured for the former irradiation geometry  $\Phi_{old} = (1.40 \pm 0.05) \times 10^8$  cm<sup>-2</sup> s<sup>-1</sup> [9] as follows:



**Fig. 1** The left picture shows the FaNGaS spectrometer with the upgraded shielding at experimental position: **1** front side of the new MEDAPP multi-leaf neutron beam collimator; **2** holder for small samples made of Teflon; **3** HPGe-detector shielding; **4** iron support

frame. The upper right picture shows the rear part of the shielding with opening doors made of BPE (borated polyethylene) to access to the detector after removing of some lead stones (down right picture)

$$\Phi_{new} = \Phi_{old} \cdot \frac{(A/h^2)_{new}}{(A/h^2)_{old}} \quad (1)$$

with  $A/h^2$  as the solid angle subtended at the neutron source by the collimated neutron beam. The value of  $\Phi_{new}$  obtained by means of Eq. (1) is  $(1.12 \pm 0.04) \times 10^8 \text{ cm}^{-2} \text{ s}^{-1}$  and corresponds to a reduction of 20% of the fast neutron flux at sample position.

The beam background spectrum measured with the new shielding of the HPGe detector is shown in Fig. 2 together with that one measured with the former shielding. The overall detector count rate is reduced by a factor of 1.5 ( $3827 \text{ s}^{-1}$  vs.  $5736 \text{ s}^{-1}$ ) and the detector dead time by a factor of 1.7 (8.59% vs. 13.59%). The count rates of the background gamma lines are reduced by factors ranging between 1.4 and 3.7 depending on their production reactions and places.

## Experimental

Prompt gamma radiation produced by interaction of fast neutrons with a calcium carbonate ( $\text{CaCO}_3$ ) powder sample of natural composition with a mass of 2.402 g (Ca: 0.962 g, C: 0.288 g, O: 1.152 g) was investigated with the FaNGaS instrument described in the section above. The powder was filled into a small PTFE (Polytetrafluorethylene) bag and compressed to a thickness of about 1 mm. The PTFE bag carrying the sample was attached to a thin PTFE rod and irradiation of the complete sample surface area was ensured by a laser-assisted alignment. The sample was tilted by an angle of  $45^\circ$  with respect to the neutron beam axis and irradiated for a total of 8.60 h. The gamma-ray spectrum was counted for 6.46 h (live time) with the electromechanically cooled coaxial HPGe detector of the FaNGaS instrument (50% relative efficiency and 2.1 keV energy resolution (FWHM) at 1.33 MeV [7]). The distance from the sample

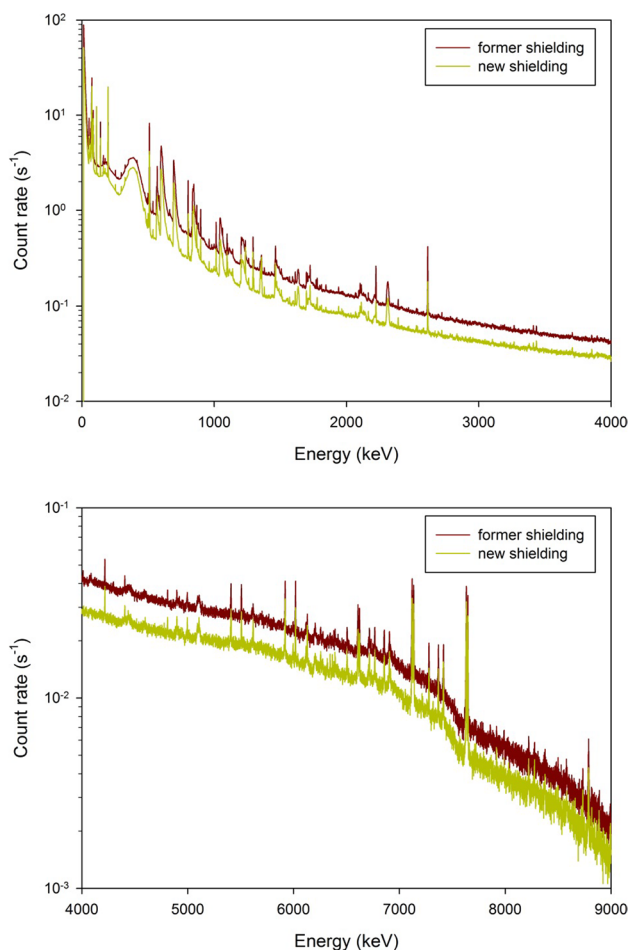


**Fig. 2** Beam background spectra measured with the new and former spectrometer shielding. The origin of prominent lines attributed to the beam background is discussed within our former publications [7, 9]

towards the detector endcap is 67 cm and the measurement was performed at an angle of  $90^\circ$  between neutron beam axis and detector. The acquired spectrum was analyzed with the HYPERMET-PC software [19] and it is shown in Figs. 3 and 4. Prompt gamma rays emitted from the  $(n, n'\gamma)$  inelastic scattering of fast neutrons as well as gamma rays induced by  $(n, p)$  and  $(n, \alpha)$  reactions were identified using the NuDat 3.0 database [20] that provides nuclear data from various evaluations for all isotopes relevant to this work [21–30]. Presence of gamma rays from  $(n, \gamma)$  reactions and possible interferences was checked with the prompt gamma neutron activation analysis (PGNAA) database [31].

Additionally, the prompt gamma-ray spectrum of the same iron foil ( $m = 1.282$  g, dimensions:  $25 \times 25 \times 0.25$  mm<sup>3</sup>) investigated with the former version of the FaNGaS instrument [9] was measured in order to determine the fast neutron flux at the sample position. In this case, the irradiation time was 15.21 h and the counting time 12.84 h (live time). The fast neutron flux was obtained by comparing the count rates of

the most intense gamma lines of  $^{56}\text{Fe}$  at 846.9, 1238.3 and 1810.9 keV induced by inelastic scattering of fast neutrons in the two experiments (Table 1). The mean value of the ratios is  $0.807 \pm 0.006$  and leads to a value of the fast neutron flux of  $(1.13 \pm 0.04) \times 10^8$  cm<sup>-2</sup> s<sup>-1</sup> which agrees very well with the value estimated from the change of the solid angle.

As a certain fraction of neutrons scatters towards the spectrometer, we have found that the count rate of lines attributed to the background is increased depending on their origin. For the calcium carbonate sample, we found a mean factor of  $2.11 \pm 0.29$  and for the iron sample a mean factor of  $1.20 \pm 0.12$ . These scattering factors were utilized to correct for interfering background lines. Possible interferences from single (SE) and double (DE) escape peaks were not identified and therefore no issue.

## Method

Inelastic scattering  $(n, n')$ ,  $(n, p)$ - and  $(n, \alpha)$ -capture reactions are induced exclusively by fast neutrons due to an associated energy threshold close to the MeV regime. The net peak area  $P_{E\gamma}$  of a prompt gamma ray induced by fast neutrons in the aforementioned reaction types can be described by the following relationship:

$$P_{E\gamma}(90^\circ) = \frac{m}{M} \cdot N_{Av} \cdot h \cdot \varepsilon_{E\gamma} \cdot \langle \sigma_{E\gamma}(90^\circ) \rangle \cdot \Phi_{fast} \cdot t_c \cdot f_n \cdot f_{E\gamma} \quad (2)$$

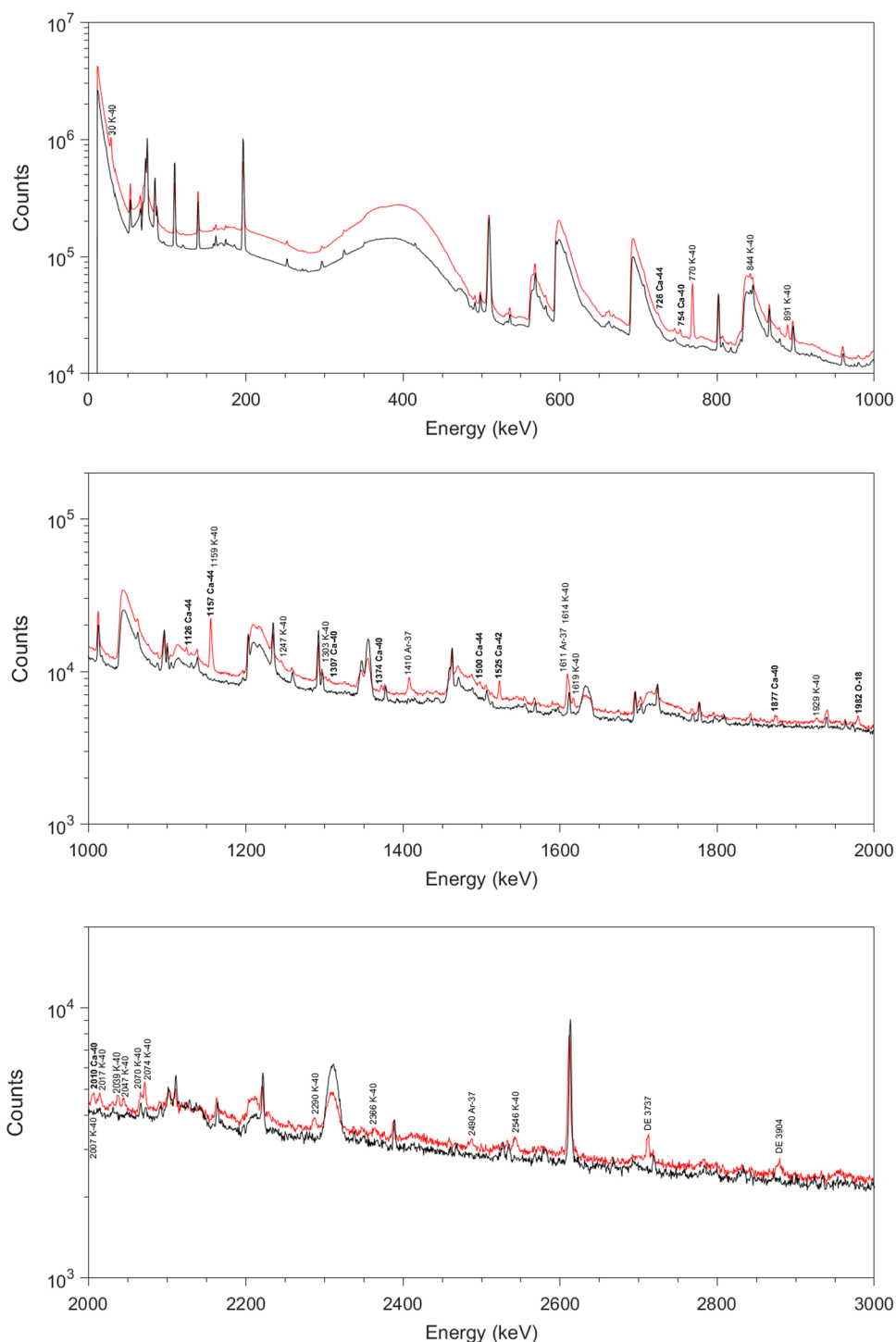
where  $m$  (g) is the mass of the considered element,  $M$  is the molar mass (g mol<sup>-1</sup>),  $N_{Av}$  the Avogadro constant ( $6.022 \times 10^{23}$  mol<sup>-1</sup>),  $h$  the isotopic abundance,  $\varepsilon_{E\gamma}$  the full-energy-peak efficiency,  $\langle \sigma_{E\gamma}(90^\circ) \rangle$  the fast neutron spectrum averaged partial gamma-ray production cross section (cm<sup>2</sup>) for an angle of  $90^\circ$  between neutron beam and detector,  $\Phi_{fast}$  the integral fast neutron flux (cm<sup>-2</sup> s<sup>-1</sup>),  $t_c$  the counting live time (s),  $f_n$  the neutron self-shielding factor and  $f_{E\gamma}$  the gamma self-absorption factor. Even tilted at an angle of  $45^\circ$  the sample is thin enough (effective thickness  $\sim 1.4$  mm) to neglect the absorption of fast neutrons, i.e.  $f_n \sim 1$  and the absorption of gamma rays with energies higher than about 100 keV, i.e.  $f_{E\gamma} \sim 1$ .

## Prompt gamma rays induced in CaCO<sub>3</sub>

In total, 38 prompt gamma ray lines were observed and identified. These gamma rays are listed in Table 2. From all 38 lines, 15 were found to belong to  $(n, n'\gamma)$ - and 20 to  $(n, p)$ - and 3 to  $(n, \alpha)$ -reactions. From the 15  $(n, n'\gamma)$  reactions 12 lines are assigned to calcium (7 for  $^{40}\text{Ca}$ , 1 for  $^{42}\text{Ca}$  and 4 for  $^{44}\text{Ca}$ ), 2 to oxygen (1 for  $^{16}\text{O}$  and 1 for  $^{18}\text{O}$ ) and 1 to carbon ( $^{12}\text{C}$ ). The  $(n, p)$  and  $(n, \alpha)$  reactions both originate from the  $^{40}\text{Ca}$  isotope, i.e. the reactions  $^{40}\text{Ca}(n, p)^{40}\text{K}$  and  $^{40}\text{Ca}(n, \alpha)^{37}\text{Ar}$ ,



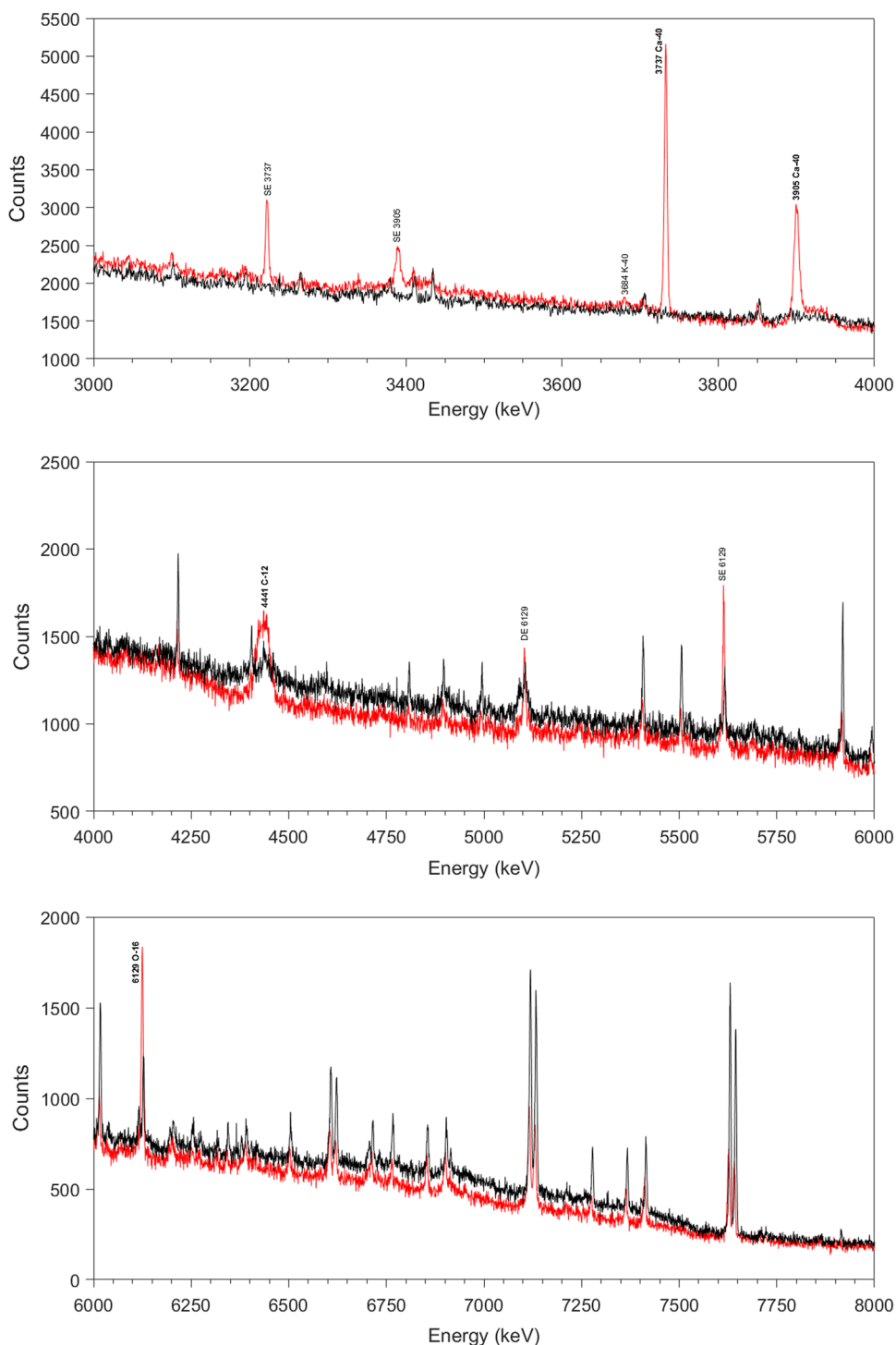
**Fig. 3** Gamma-ray spectra in the energy range 0–3000 keV acquired during 23,240 s counting live time for the calcium sample (red) and during 51,506 s for the beam background (black). Prompt gamma rays induced by (n,p) reactions (K-40) and (n, $\alpha$ ) reactions (Ar-37) are written in black. Prompt gamma rays issued from (n,n') inelastic scattering of fast neutrons are written in bold. Abbreviations SE and DE indicate single and double escape peaks, respectively. The origin of prominent lines attributed to the beam background is discussed within our former publications [7, 9]



respectively. As relative light nuclei, calcium, carbon and oxygen are potentially subject to Doppler broadening [32]. The line at 3904.8 keV from the  $^{40}\text{Ca}(n,n'\gamma)^{40}\text{Ca}$  reaction and the line at 4441.1 keV from the  $^{12}\text{C}(n,n'\gamma)^{12}\text{C}$  reaction show a broadening because the gamma rays are emitted in flight, i.e. the time scale of the nuclear lifetime of the respective excited states is smaller ( $\sim$ fs [20, 33]) than the stopping process of the recoiling nucleus. The gamma line at

6129.3 keV originating from the  $^{16}\text{O}(n,n'\gamma)^{16}\text{O}$  reaction interferes with the decay line of  $^{16}\text{N}$  ( $E_\gamma = 6128.6$  keV,  $I_\gamma = 67.0\%$ ,  $t_{1/2} = 7.13$  s [34]), that is formed via the  $^{16}\text{O}(n,p)^{16}\text{N}$  reaction. However, the interference can be neglected since the cross section (fission spectrum average for  $kT = 1.35$  MeV, taken from [35]) of the  $^{16}\text{O}(n,p)^{16}\text{N}$  reaction ( $44.72$   $\mu\text{b}$  [35]), is considerably lower than that of the  $^{16}\text{O}(n,n'\gamma)^{16}\text{O}$  reaction ( $4.92$  mb [35]) and its contribution to the net count rate is

**Fig. 4** Gamma-ray spectra in the energy range 3000–8000 keV acquired during 23,240 s for the calcium sample (red) and during 51,506 s for the beam background (black). Prompt gamma rays induced by (n,p) reactions (K-40) are written in black. Prompt gamma rays issued from (n,n') inelastic scattering of fission neutrons are written in bold. Abbreviations SE and DE indicate single and double escape peaks, respectively. The origin of prominent lines attributed to the beam background is discussed within our former publications [7, 9]



only  $1.36 \pm 0.20\%$ . Intensities of gamma lines were calculated relative to the 3905-keV line (100%,  $^{40}\text{Ca}$ ) for calcium and to the 1982-keV line (100%,  $^{18}\text{O}$ ) for oxygen, both emitted from the (n,n' $\gamma$ ) reaction of the first low-lying  $2^+$  states. Relative intensities are given along with the values determined in [16] in columns 4 and 7 of Table 2. In order to support the discussion of obtained results, Table 2 also contains

the reaction thresholds taken from [36, 37] for each reaction in column 1 in brackets and Fig. 5 shows the neutron energy spectrum of the FaNGaS instrument as described in this work together with the neutron energy dependence of the grouped microscopic cross sections averaged over each neutron energy bin for every reaction that we have observed. Grouped cross sections were obtained by processing nuclear

**Table 1** Count rates (*CR*) of the three most intense gamma lines of  $^{56}\text{Fe}$  produced by inelastic scattering of fast neutrons measured from the same iron foil with the old and new version of the FaNGaS instrument. The distance between the foil and the detector was identical (67 cm) for the two measurements

$E_\gamma$ (keV)	$CR_{old}$ ( $s^{-1}$ )	$CR_{new}$ ( $s^{-1}$ )	$CR_{new}/CR_{old}$
846.9	$156 \pm 6$	$126 \pm 7$	$0.81 \pm 0.05$
1238.3	$12.5 \pm 0.6$	$10.0 \pm 0.4$	$0.80 \pm 0.05$
1810.8	$5.9 \pm 0.4$	$4.8 \pm 0.3$	$0.81 \pm 0.07$

data from the latest evaluated nuclear data file (ENDF) library (ENDF/B-VIII.0 [38]) with the NJOY Nuclear Data Processing System (Version 2016) [39, 40]. In comparison to [16], we have observed 32 from 38 listed lines resulting from the reaction of fast neutrons. All lines of carbon and oxygen were observed. For calcium, lines listed at energies of 1345.6, 1369.5, 2951.9, 5250, 5628 and 5902 keV, respectively, were not observed in our measurement. According to NuDat 3.0 [20], the lines at 1345.6 and 5250 keV belong to the same excited level ( $E^* = 5248.8$  keV) of the  $^{40}\text{Ca}(n,n'\gamma)^{40}\text{Ca}$  reaction. As depicted in Fig. 5 and as given in [36, 37], the energy threshold of this reaction is around 3.44 MeV, which is already above our mean neutron energy of 2.30 MeV. Our integral fast neutron flux is defined for an energy range of  $60 \text{ keV} \leq E_n \leq 20 \text{ MeV}$ , but with respect to Fig. 5 the effective activation flux, integrated over the limits of the cross-section curve, is  $(2.19 \pm 0.08) \times 10^7 \text{ cm}^{-2} \text{ s}^{-1}$ . This shows that only 19.4% of our defined fast neutron flux of  $(1.13 \pm 0.04) \times 10^8 \text{ cm}^{-2} \text{ s}^{-1}$  is able to induce inelastic scattering in  $^{40}\text{Ca}$ . Although Demidov et al. have a smaller mean neutron energy (0.631 MeV), they have irradiated a much higher calcium mass (11.3 g [16] vs. 0.962 g in this work) for a longer time (24.2 h [16] vs 6.46 h counting live time). Therefore, it might be possible that the detection limit was not reached in our measurement. The evaluated nuclear structure data (ENSDF) file of the  $(n,n'\gamma)$  reaction of  $^{40}\text{Ca}$  from [41] available on [20] gives differential cross sections  $d\sigma/d\Omega$  for a measuring angle of  $125^\circ$  and several discrete neutron energies between 4.85 and 8.05 MeV. From our iron measurement [9] we can observe that the correction for the anisotropy becomes negligible for high-energy lines, i.e. the angular distribution factor  $W(125^\circ)/W(90^\circ) \approx 1$ . For the energy range between 6.45 to 8.05 MeV in [41], the ratio in percent of differential cross sections between the lines at 5250 and 3905 keV is  $21.8 \pm 6.4\%$ , which agrees well with the relative intensity of  $27 \pm 5\%$  from [16]. Therefore, even though the gamma-ray spectrum is not shown beyond 3 MeV in [16] and the relative intensity of the 5250-keV line is in the range of other lines clearly observed, we can assume that Demidov et al. have seen this line due to their higher irradiated mass. The line listed at 1369.5 keV is unassigned in the Demidov

Atlas and belongs probably to the background as we have not identified a peak with significant statistics and the evaluated nuclear data in NuDat 3.0 does not propose a reasonable corresponding transition. The gamma ray listed at 2951.9 keV is also unassigned by Demidov et al. and might be another mistake as again no transition is found in NuDat 3.0. Curiously, in the visual excerpt of their spectrum this line is neither seen nor marked accordingly. The gamma-ray peaks at 5628 and 5902 keV both belong to the  $^{40}\text{Ca}(n,n'\gamma)^{40}\text{Ca}$  reaction [20, 25] and should be present in the spectrum from Demidov et al. due to the higher irradiated mass and longer exposure time. Presence of these lines in [16] is supported as the differential cross-section ratios [41] relative to the 3905-keV line are  $14.8 \pm 3.2\%$  (5628 keV) and  $9.6 \pm 3.2\%$  (5902 keV), respectively, which is under consideration of the large errors in well agreement to the relative intensities of  $21 \pm 5\%$  and  $16 \pm 5\%$  given in [16]. Nevertheless, these lines require high excitation energies above 5 MeV and in principle one would expect to observe such lines better in our measurement due to the higher mean neutron energy (2.30 MeV vs. 0.631 MeV).

On the other hand, compared to [16] also 6 new gamma lines related to calcium were identified. The line at 1613.58 keV from the  $^{40}\text{Ca}(n,p)^{40}\text{K}$  reaction was probably unresolved by Demidov et al. due to the worse detector resolution and the close-lying line at 1611.24 keV coming from the  $^{40}\text{Ca}(n,\alpha)^{37}\text{Ar}$  reaction. According to [31] the line at 2009.76 keV could arise from the  $^{40}\text{Ca}(n,\gamma)^{41}\text{Ca}$  reaction, but as stronger capture lines were not observed we exclude this possibility. In [25] available on NuDat 3.0 [20] a transition of 2009.5 keV for the isotope  $^{40}\text{Ca}$  induced by a  $(p,p'\gamma)$  reaction [42] from a level at 7623.11 keV is proposed. In view of this high excitation energy and also 12 MeV neutron energy used in [42] with respect to our neutron spectrum we do not find the aforementioned transition reasonable, rather we cautiously assign this line to the  $^{40}\text{Ca}(n,n'\gamma)^{40}\text{Ca}$  reaction assuming that it might be a transition not captured in NuDat 3.0 yet. The low-energy gamma ray at 29.77 keV from the  $^{40}\text{Ca}(n,p)^{40}\text{K}$  reaction could not be detected by Demidov et al. since the measurement was limited to gamma-ray energies down to 120 keV [16]. The line at 2289.7 keV was assigned to the  $^{40}\text{Ca}(n,p)^{40}\text{K}$  reaction, although according to NuDat 3.0 [20, 25] it might be also fed by the inelastic scattering reaction in  $^{40}\text{Ca}$ . However, with respect to Fig. 5 we assume the contribution of inelastic scattering to be negligible since the required excitation energy ( $E^* = 6025.5$  keV [20, 25]) is far above our neutron mean energy of 2.30 MeV.

The line at 29.77 keV was corrected for gamma self-absorption analytically with the following relationship [31]:

$$f_{E\gamma} = \frac{1 - e^{-\frac{\mu}{\rho} \cdot \rho \cdot l}}{\frac{\mu}{\rho} \cdot \rho \cdot l} \quad (3)$$

**Table 2** Prompt gamma rays of calcium, carbon and oxygen induced by fast neutrons on CaCO<sub>3</sub>

Reaction ( $E_{thr}$ )	This work				From Demidov Atlas [16]		$R$
	$E_\gamma$ (keV)	$(P_{E_\gamma}(90^\circ)/\epsilon_{E_\gamma}) \times 10^{-8}$ (count)	$I_R$ (relative) (%)	$\langle \sigma_{E_\gamma}(90^\circ) \rangle$ (mb)	$E_\gamma$ (keV)	$I_R$ (relative) (%)	
$^{40}\text{Ca}(n,n'\gamma)^{40}\text{Ca}$ (3.44 MeV)	754.41 ± 0.07	0.53 ± 0.03	13.5 ± 0.9	1.45 ± 0.14	755.0 ± 0.4	15 ± 3	-0.48
	1307.49 ± 0.26	0.16 ± 0.03	3.93 ± 0.88	0.42 ± 0.10	–	–	–
	1374.32 ± 0.13 <sup>a</sup>	0.36 ± 0.03	8.99 ± 0.89	0.97 ± 0.12	1375.7 ± 1.0	10 ± 2	-0.46
	1876.91 ± 0.19	0.35 ± 0.04	8.78 ± 1.09	0.95 ± 0.13	1877.5 ± 0.9	7.8 ± 1.2	0.61
	2009.76 ± 0.23 <sup>b</sup>	0.28 ± 0.04	6.96 ± 0.95	0.75 ± 0.12	–	–	–
	3736.89 ± 0.13	5.28 ± 0.17	133 ± 6	14.3 ± 1.2	3736.9 ± 0.8	123 ± 9	0.93
	3904.76 ± 0.28 <sup>c</sup>	3.96 ± 0.14	100	10.8 ± 0.9	3904.2	100	–
$^{42}\text{Ca}(n,n'\gamma)^{42}\text{Ca}$ (1.56 MeV)	1524.62 ± 0.07	0.87 ± 0.05	22.1 ± 1.4	355 ± 34	1524.4 ± 0.4	20 ± 3	0.63
$^{44}\text{Ca}(n,n'\gamma)^{44}\text{Ca}$ (1.18 MeV)	726.17 ± 0.11	0.50 ± 0.07	12.5 ± 1.9	46 ± 8	726.3 ± 1.0	12 ± 3	0.14
	1126.03 ± 0.11	0.34 ± 0.03	8.51 ± 0.85	31 ± 4	1125.5 ± 1.0	8.2 ± 2.0	0.14
	1156.78 ± 0.05	3.90 ± 0.14	98 ± 5	359 ± 31	1156.9 ± 0.5	87 ± 6	1.48
$^{40}\text{Ca}(n,p)^{40}\text{K}$ (0.54 MeV)	1499.88 ± 0.28	0.21 ± 0.04	5.38 ± 0.93	19.6 ± 3.7	1500.6 ± 0.8	4.6 ± 1.2	0.52
	29.78 ± 0.05	63 ± 4 <sup>d</sup>	1589 ± 121	171 ± 18	–	–	–
	769.89 ± 0.07 <sup>a</sup>	9.56 ± 0.29	241 ± 41	26 ± 2	770.3 ± 0.2	204 ± 10	2.49
	843.54 ± 0.06 <sup>a</sup>	0.86 ± 0.15	21.7 ± 3.9	2.34 ± 0.45	–	–	–
	891.19 ± 0.05	1.66 ± 0.07	42 ± 2	4.52 ± 0.41	891.6 ± 0.4	59 ± 7	-2.30
	1158.93 ± 0.10	0.83 ± 0.06	20 ± 2	2.27 ± 0.23	1159.1 ± 0.8	26 ± 4	-1.15
	1247.29 ± 0.16	0.27 ± 0.03	6.77 ± 0.90	0.73 ± 0.11	1247.5 ± 0.6	7.5 ± 2.2	-0.31
	1302.88 ± 0.18	0.27 ± 0.04	6.76 ± 0.93	0.73 ± 0.11	1303.0 ± 0.6	8.1 ± 2.0	-0.61
	1613.58 ± 0.12 <sup>a</sup>	0.04 ± 0.01	1.06 ± 0.17	0.11 ± 0.02	–	–	–
	1618.68 ± 0.15	0.39 ± 0.04	9.89 ± 1.08	1.06 ± 0.14	1616.8 ± 1.0 <sup>e</sup>	17 ± 4	-1.72
	1929.02 ± 0.22	0.17 ± 0.03	4.29 ± 0.66	0.46 ± 0.08	1929.2 ± 1.6	6.1 ± 1.0	-1.51
	2007.13 ± 0.30	0.22 ± 0.04	5.43 ± 0.92	0.58 ± 0.11	2007.8 ± 0.9 <sup>f</sup>	8.3 ± 1.3	-1.80
	2017.39 ± 0.21 <sup>a</sup>	0.17 ± 0.05	4.40 ± 1.20	0.47 ± 0.13	2017.8 ± 0.9	5.8 ± 1.2	-0.82
	2039.49 ± 0.19	0.38 ± 0.04	9.68 ± 1.00	1.04 ± 0.13	2040.4 ± 1.0	8.0 ± 1.3	1.02
	2046.72 ± 0.24	0.29 ± 0.04	7.43 ± 0.95	0.80 ± 0.12	2047.8 ± 1.5	4.8 ± 1.1	1.81
	2069.85 ± 0.30	0.32 ± 0.04	7.99 ± 1.15	0.86 ± 0.14	2068.3 ± 1.6	6.0 ± 1.2	1.20
	2073.55 ± 0.12 <sup>a</sup>	0.45 ± 0.08	11.3 ± 2.1	1.22 ± 0.24	2073.4 ± 1.0	13 ± 2	-0.57
	2289.66 ± 0.21 <sup>g</sup>	0.28 ± 0.02	6.95 ± 0.67	0.75 ± 0.09	2289.8 ± 1.2	11 ± 2	-1.92
	2366.25 ± 0.50	0.18 ± 0.04	4.54 ± 0.98	0.49 ± 0.11	2366.6 ± 2.0	4.8 ± 1.0	-0.19
	2545.64 ± 0.27	0.52 ± 0.06	13.2 ± 1.5	1.42 ± 0.19	2545.1 ± 1.0	14 ± 2	-0.31
3683.79 ± 0.37	0.16 ± 0.03	4.15 ± 0.71	0.45 ± 0.08	–	–	–	
$^{40}\text{Ca}(n,\alpha)^{37}\text{Ar}$ (0 MeV)	1409.61 ± 0.10 <sup>a</sup>	0.74 ± 0.04	18.8 ± 1.1	2.02 ± 0.19	1409.8	21 ± 3	-0.70
	1611.24 ± 0.08	1.65 ± 0.07	42 ± 2	4.47 ± 0.40	1611.2 ± 0.6 <sup>h</sup>	48 ± 5	-0.95
	2490.24 ± 0.27	0.17 ± 0.03	4.41 ± 0.73	0.47 ± 0.08	2490.0 ± 1.0	9 ± 2	-2.16
$^{12}\text{C}(n,n'\gamma)^{12}\text{C}$ (4.81 MeV) <sup>j</sup>	4441.14 ± 0.42 <sup>a,c</sup>	5.39 ± 1.14	100	14.4 ± 3.3	4438 ± 2	109 <sup>i</sup>	–
$^{16}\text{O}(n,n'\gamma)^{16}\text{O}$ (6.43 MeV) <sup>j</sup>	6129.32 ± 0.22 <sup>a</sup>	2.50 ± 0.37	547 ± 121	2.20 ± 0.37	6129.3 ± 1.0	595 ± 120	-0.28
$^{18}\text{O}(n,n'\gamma)^{18}\text{O}$ (6.43 MeV) <sup>j</sup>	1981.69 ± 0.18	0.46 ± 0.05	100	201 ± 28	1983.0 ± 0.4	100	–

$E_{thr}$  is the threshold energy of the considered reaction taken from [36, 37],  $E_\gamma$  is the gamma-ray energy,  $(P_{E_\gamma}(90^\circ)/\epsilon_{E_\gamma}) \times 10^{-8}$  the net counts in the gamma-ray peak divided by the full-energy-peak efficiency,  $I_R$  the relative intensity of the gamma ray and  $\langle \sigma_{E_\gamma}(90^\circ) \rangle$  the fission neutron spectrum averaged isotopic partial cross section for gamma-ray production at an angle of 90° between neutron beam and detector determined with Eq. (2).  $R$  is the residual calculated by means of Eq. (5)

<sup>a</sup>Corrected for background interferences

<sup>b</sup> $^{40}\text{Ca}(n,\gamma)^{41}\text{Ca}$  excluded and no clear identification in NuDat 3.0 [20], cautious assumption. With regard to our neutron spectrum, it is questionable if this line really comes from the high level at 7623.11 keV or if it is a transition not captured in NuDat 3.0 yet

<sup>c</sup>Doppler-broadened

<sup>d</sup> $(P_{E_\gamma})/(\epsilon_{E_\gamma} \cdot f_{E_\gamma})$  with  $f_{E_\gamma} = 0.731 \pm 0.022$ , i.e. gamma self-absorption calculated after Eq. (3) with data from NIST XCOM [43]

<sup>e</sup>Wrong level energy assigned by Demidov et al.



**Table 2** (continued)

<sup>f</sup>Cautious assumption that this is our line from the  $^{40}\text{Ca}(n,p)^{40}\text{K}$  reaction due to a relatively low excitation level energy of 2807.88 keV and well agreement to peak energy of 2007.71 keV given in [20, 25]. Despite roughly 2 keV difference in energy, it might also be the same line as observed by us at 2009.76 keV assigned to the  $^{40}\text{Ca}(n,n'\gamma)^{40}\text{Ca}$  reaction as the uncertainty is high and the relative intensities are comparable

<sup>g</sup>Weak interference from the  $^{40}\text{Ca}(n,n'\gamma)^{40}\text{Ca}$  reaction possible

<sup>h</sup>1611 and 1614 keV

<sup>i</sup>Unclear how this intensity is obtained, it might be a mistake or the absolute intensity determined with the integral cross section. From our work the absolute intensity is 120% by using an integral cross section for fission neutrons of 12 mb with  $W(90^\circ)=1$

<sup>j</sup>Only elemental data available from [36, 37]

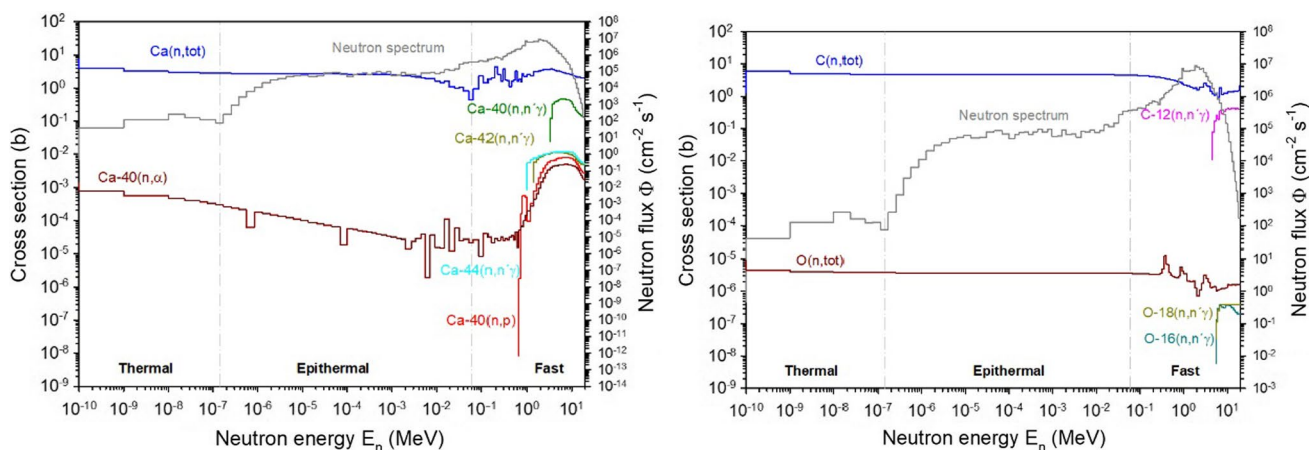


**Fig. 5** Neutron energy spectrum of the modified FaNGaS version as described within this work at sample position (right scale of y-axis) and neutron energy dependence of the grouped microscopic cross sections  $\sigma_i(E)$  averaged over the neutron energy bin  $i$  (left scale of

y-axis) for total (n,tot), fast neutron inelastic scattering (n,n'), (n,p) and (n,α) reactions for calcium (left side) and carbon and oxygen (right side). Values of the (n,tot) reactions were obtained by summing isotopic values in each energy bin weighted with isotopic abundances

where  $l$  (cm) is the effective thickness of the sample,  $\mu/\rho$  ( $\text{cm}^2 \text{g}^{-1}$ ) denotes the mass attenuation coefficient ( $\text{cm}^2 \text{g}^{-1}$ ) and  $\rho$  ( $\text{g cm}^{-3}$ ) is the density of the sample (for  $\text{CaCO}_3$ ,  $\rho = 2.71 \text{ g cm}^{-3}$ ). Neglecting coherent scattering, the value of  $\mu/\rho$  was taken from NIST (National Institute of Standards and Technology) photon cross sections database XCOM [43]. To account for the uncertainty in thickness related to the powder nature of the sample, an error of 10% was applied to the thickness. A calculated value of  $f_{E\gamma} = 0.731 \pm 0.022$  indicates an attenuation of the 29.77-keV gamma rays by ~27%. For the gamma ray of second-lowest energy, the 726.2-keV line from the  $^{44}\text{Ca}(n,n'\gamma)^{44}\text{Ca}$  reaction,  $f_{E\gamma} = 0.986 \pm 0.001$ . Therefore, gamma self-absorption can be neglected for all observed gamma rays except the one at 29.77 keV.

The relationship between the relative intensities measured in this work and those given in [16] is depicted in Fig. 6 for all lines originating from calcium. The values have been fitted with the following semi-empirical function:

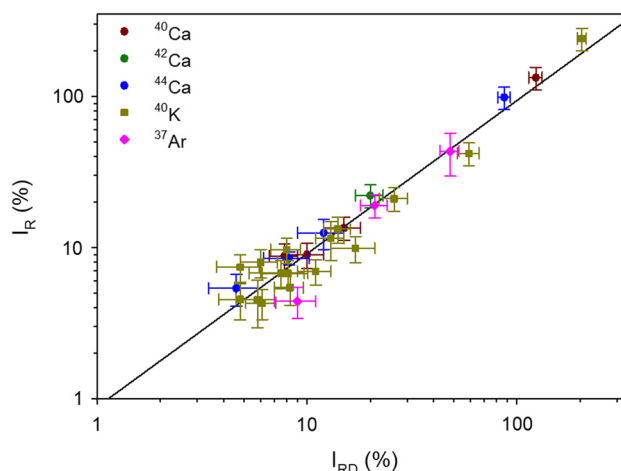


**Fig. 6** Relationship between the relative intensities  $I_R$  of the prompt gamma rays induced by fast neutron inelastic scattering (n,n'), (n,p) or (n,α) reactions on calcium measured in this work and the relative intensities  $I_{RD}$  tabulated in the Demidov Atlas [16]. The solid line represents the fit of the data with Eq. (4)

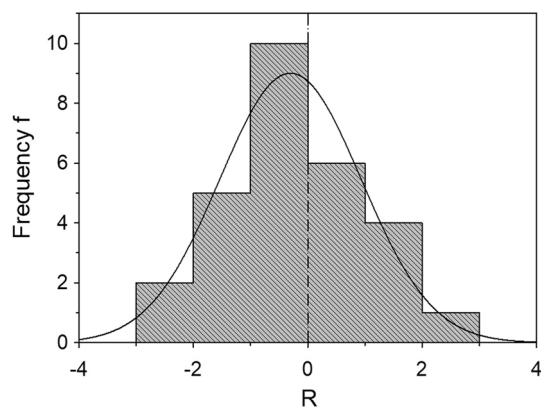


**Fig. 7** Comparison of the relative intensities of the prompt gamma rays induced by fast neutron inelastic scattering (n,n'), (n,p) and (n, $\alpha$ ) reactions on calcium obtained in this work with the data tabulated in the Demidov Atlas [16] in the form of a histogram of the residuals  $R$  in units of standard deviation [ $\sigma$ ] calculated with Eq. (5). The values of  $R$  are given in column 8 of Table 2. The solid line represents the fit of the data with a Gaussian

$$I_R = a \cdot (I_{RD})^b \quad (4)$$

with  $a = 0.88 \pm 0.13$  and  $b = 1.01 \pm 0.05$ .

The average intensity ratio  $I_R/I_{RD}$  of  $0.94 \pm 0.23$  indicates a rather good agreement between the two measurements. To prove the consistency in a more detailed manner, Fig. 7 shows the two sets of data in the form of a histogram of the residuals  $R$  in units of standard deviation [ $\sigma$ ], calculated as:

$$R = \frac{I_R - I_{RD}}{\sqrt{(s_{I_R})^2 + (s_{I_{RD}})^2}} \quad (5)$$

The fit of the data agrees at the  $1.2\sigma$  level and the Gaussian centroid is shifted by  $-0.302$ , indicating a probable systematic effect. The fast neutron spectrum averaged isotopic cross sections for gamma-ray production calculated by means of Eq. (2) with a fast neutron flux of  $(1.13 \pm 0.04) \times 10^8 \text{ cm}^{-2} \text{ s}^{-1}$  are given in column 5 of Table 2.

### Detection limit

The detection limit (DL) might be defined as the minimum mass of a pure element that has to be irradiated for a certain time in order to give a net signal above the background with a certain standard deviation  $\sigma$ . For a certain counting live time  $t_c$  and neglecting any neutron and gamma beam attenuation effects, it can be calculated with Eq. (2) from the minimum peak area  $P_{E\gamma}(c)$  that might be estimated according to [44] as:

$$P_{E\gamma}(c) = \frac{\sqrt{2 \cdot B_{E\gamma}}}{c} \quad (6)$$

where  $B_{E\gamma}$  is the area of the background below the gamma line of interest and  $c$  a predefined value for the relative uncertainty of the peak area. In the presence of an interfering peak  $P_{E\gamma}(c)$  can be expressed as:

$$P_{E\gamma}(c) = \frac{\sqrt{2 \cdot (P_{int} + 2 \cdot B_{E\gamma})}}{c} \quad (7)$$

where  $P_{int}$  is the net area of the interfering peak.

For a counting live time of 12 h, the DL of calcium, carbon and oxygen were calculated for the most intense gamma line of each element by means of Eqs. (2), (6) and (7). The value of  $B_{E\gamma}$  was determined from the beam background with HYPERMET-PC. For a value of  $c = 0.5$ , corresponding to a peak area uncertainty of 50%, the smallest quantity of pure element that can be detected is 5 mg for calcium ( $^{40}\text{Ca}$ ,  $E_\gamma = 29.8 \text{ keV}$ ,  $\langle \sigma_{E\gamma}(90^\circ) \rangle = 171 \text{ mb}$ ), 13 mg for carbon ( $^{12}\text{C}$ ,  $E_\gamma = 4441.1 \text{ keV}$ ,  $\langle \sigma_{E\gamma}(90^\circ) \rangle = 14.4 \text{ mb}$ ) and 64 mg for oxygen ( $^{16}\text{O}$ ,  $E_\gamma = 6129.3 \text{ keV}$ ,  $\langle \sigma_{E\gamma}(90^\circ) \rangle = 2.20 \text{ mb}$ ). It is worth mentioning that, in contrast to carbon and oxygen, the detection limit for calcium is derived from the (n,p) rather than the (n,n') reaction. With respect to Fig. 5 this is reasoned in a lower reaction threshold, i.e. a greater overlap between the fast neutron spectrum and the cross-section curve.

### Conclusions

A new version of the FaNGaS instrument operated at MLZ is presented. The shielding of the gamma-ray detector was upgraded in order to improve the beam background as well as to facilitate the access to the detector. Compared to the previous shielding the total background count rate was decreased by a factor of 1.5 and the count rates of background lines by factors ranging between 1.4 and 3.7 depending on their origins. Additionally, due to the new MLC of the MEDAPP facility, the distance between the sample and the neutron source (uranium converter plate) was increased leading to a reduction by 20% of the fast neutron flux at irradiation position compared to the previous geometry ( $1.13 \times 10^8 \text{ cm}^{-2} \text{ s}^{-1}$  vs.  $1.40 \times 10^8 \text{ cm}^{-2} \text{ s}^{-1}$ ). As the composition of the new MLC potentially enables moderation processes, the thermal and epithermal neutron flux might be increased at the sample position. This will be investigated in a future work as only fast neutrons were relevant for the present work.

The emission of prompt gamma rays in calcium, carbon and oxygen from (n,n'), (n,p) and (n, $\alpha$ ) reactions was investigated by irradiating a  $\text{CaCO}_3$  sample. Gamma rays

were recorded at an angle of 90° between the FaNGaS spectrometer and the fast neutron beam.

In total, 38 prompt gamma rays were observed. From these, 20 gamma lines were assigned to the  $^{40}\text{Ca}(n,p)^{40}\text{K}$  reaction, 15 lines to  $(n,n'\gamma)$  reactions (12 in Ca, 1 in C and 2 in O) and another 3 to the  $^{40}\text{Ca}(n,\alpha)^{37}\text{Ar}$  reaction. Relative intensities and fast neutron spectrum averaged isotopic gamma-ray production cross sections were determined and compared to the work of Demidov et al. [16]. Intensities of calcium lines were calculated relative to the 3905-keV line (100%) of  $^{40}\text{Ca}$  and the intensities of oxygen lines were calculated relative to the 1982-keV line (100%) of  $^{18}\text{O}$ . Compared to [16], 6 gamma lines of calcium were not observed in our measurement probably due to the lower sample mass and measuring time. On the other hand some gamma rays given in [16] are probably false identifications as they are not mentioned in NuDat 3.0 [20]. Apart from that, we have observed 6 new gamma rays compared to [16], thanks to our better detector resolution and higher mean excitation energy (2.30 MeV). The relative intensities of the calcium lines measured in our work agree well ( $1.2\sigma$  level) with the values given in [16]. The detection limits of calcium, carbon and oxygen are 5, 13 and 64 mg, respectively, for a counting time of 12 h.

**Acknowledgements** The reconstruction of the instrument by Johannes Pfeil and Linus Willerding from the Infrastructure group of FRM II is acknowledged.

**Funding** Open Access funding enabled and organized by Projekt DEAL.

## Declarations

**Conflict of interest** The authors have no conflict of interest to declare that are relevant to the content of this article.

**Open Access** This article is licensed under a Creative Commons Attribution 4.0 International License, which permits use, sharing, adaptation, distribution and reproduction in any medium or format, as long as you give appropriate credit to the original author(s) and the source, provide a link to the Creative Commons licence, and indicate if changes were made. The images or other third party material in this article are included in the article's Creative Commons licence, unless indicated otherwise in a credit line to the material. If material is not included in the article's Creative Commons licence and your intended use is not permitted by statutory regulation or exceeds the permitted use, you will need to obtain permission directly from the copyright holder. To view a copy of this licence, visit <http://creativecommons.org/licenses/by/4.0/>.

## References

- Schrader CD, Stinner RJ (1961) Remote analysis of surfaces by neutron-gamma-ray inelastic scattering techniques. *J Geophys Res* 66:1951–1956
- Jiggins AH, Habbani FI (1976) Prompt gamma-ray analysis using 3.29 MeV neutron inelastic scattering. *Int J Appl Radiat Isot* 27:689–693
- Yates SW, Filo AJ, Cheng CY, Coope DF (1978) Elemental analysis by gamma detection following inelastic neutron scattering. *J Radioanal Nucl Chem* 46:343–355
- Sowerby BD (1979) Elemental analysis by neutron inelastic scatter gamma rays with a radioisotope source. *Nucl Instrum Methods* 166:571–579
- Ahmed MR, Demidov AM, Al-Najjar SA, Al-Amili MA (1974) Use of spectroscopy of gamma-radiation from the inelastic scattering of reactor fast neutrons for elemental analysis. *J Radioanal Nucl Chem* 23:199–203
- Rossbach M, Genreith C, Randriamalala T, Mauerhofer E, Zs R, Kudejova P, Söllradl S, Belgya T, Szentmiklosi L, Firestone RB, Hurst AM, Bernstein L, Sleaford B, Escher JE (2015) TANDEM: a mutual cooperation effort for transactinide nuclear data evaluation and measurement. *J Radioanal Nucl Chem* 304:1359–1363
- Randriamalala TH, Rossbach M, Mauerhofer E, Zs R, Söllradl S, Wagner FM (2016) FaNGaS: A new instrument for  $(n, n'\gamma)$  reaction measurements at FRM II. *Nucl Instrum Methods A* 806:370–377
- Hable A, Ramsel C, Jericha E, Böck H, Randriamalala TH, Rossbach M (2017) FaNGaS: Determination of integral fast fission cross sections  $(n, f)$  of  $^{238}\text{U}$ ,  $^{237}\text{Np}$ , and  $^{242}\text{Pu}$  in a directed fission neutron beam at FRM II Garching. *J Radioanal Nucl Chem*. <https://doi.org/10.1007/s10967-017-5512-7>
- Ilic Z, Mauerhofer E, Stieghorst C, Zs R, Rossbach M, Randriamalala TH, Brückel T (2020) Prompt gamma rays induced by inelastic scattering of fission neutrons on iron. *J Radioanal Nucl Chem* 325:641–645
- Mauerhofer E, Ilic Z, Stieghorst C, Zs R, Rossbach M, Li J, Randriamalala TH, Brückel T (2021) Prompt and delayed gamma rays induced by epithermal and fast neutrons with indium. *J Radioanal Nucl Chem* 331:535–546
- Wagner F, Kneschaurek P, Kastenmüller A, Loeper-Kabasakal B, Kampfer S, Breitzkreutz H, Waschkowski W, Molls M, Petry W (2009) The munich fission neutron therapy facility MEDAPP at the research reactor FRM II. *Strahlenther Onkol*. <https://doi.org/10.1007/s00066-008-1878-3>
- Bernstein L, Brown D, Basunia S, Hurst A, Kawano T, Kelley J, Kondev F, McCutchan E, Nesaraja C, Slaybaugh R, Sonzogni A, (2015) Nuclear data needs and Capabilities for Applications, White paper LLNL Report LLNL-CONF-676585, <http://bang.berkeley.edu/events/ndnca/whitepaper>
- Romano C, Ault T, Bernstein L, Bahrn R, Talou P, Quiter B, Pozzi S, Devlin M, Burke J, Bredeweg T, McCutchan E, Stave S, Bailey T, Hogle S, Chapman C, Hurst A, Nelson N, Tovesson F, Hornback D, (2018) Proceedings of the nuclear data road-mapping and enhancement workshop (NDREW) for nonproliferation, In: White paper ORNL/LTR-2018/510, [https://www.nndc.bnl.gov/nndcscr/documents/ndrew/NDREWProc\\_FINAL.pdf](https://www.nndc.bnl.gov/nndcscr/documents/ndrew/NDREWProc_FINAL.pdf)
- Bernstein L, Romano C, Brown D, Casperson R, Descalle MA, Devlin M, Pickett C, Rearden B, Vermeulen C, (2019) Final report for the workshop for applied nuclear Data activities (WANDA), White Paper LLNL-PROC-769849
- Hurst AM, Bernstein LA, Kawano T, Lewis AM, Song K (2021) The Baghdad Atlas: a relational database of inelastic neutron scattering  $(n, n'\gamma)$  data. *Nucl Instrum Meth A* 995:165095
- Demidov A, Govor L, Cherepantsev M, Ahmed S, Al-Najjar M, Al-Amili N, Al-Assafi N, Rammo N (1978) Atlas of gamma-ray spectra from the inelastic scattering of reactor fast neutrons. Atomizdat, Moscow

17. Private communication with Dr. Tobias Chemnitz, Instrument responsible for MEDAPP at Forschungs-Neutronenquelle Heinz Maier-Leibnitz (FRM II), Garching
18. German institute for standardization (DIN) (2004) DIN 17640–1 Lead alloys for general purposes
19. Zs R, Belgya T, Molnár GL (2005) Application of Hypermet-PC in PGAA. *J Radioanal Nucl Chem* 265:261–265
20. NuDat 3.0 National Nuclear Data Center, Brookhaven National Laboratory <https://www.nndc.bnl.gov/nudat3/>
21. Kelley JH, Purcell JE, Sheu CG (2017) Energy levels of light nuclei A= 12. *Nucl Phys A* 968:71–253
22. Ajzenberg-Selove F (1991) Energy levels of light nuclei A= 13–15. *Nucl Phys A* 523:1–196
23. Tilley DR, Weller HR, Cheves CM (1993) Energy levels of light nuclei A= 16–17. *Nucl Phys A* 564:1–183
24. Tilley DR, Weller HR, Cheves CM, Chasteler RM (1995) Energy level of light nuclei A= 18–19. *Nucl Phys A* 595:1–170
25. Chen J (2017) Nuclear data sheets for A= 40. *Nucl Data Sheets* 140:1–376
26. Singh B, Chen J (2015) Nuclear data sheets for A= 43. *Nucl Data Sheets* 126:1–150
27. Chen J, Singh B, Cameron JA (2011) Nuclear data sheets for A= 44. *Nucl Data Sheets* 112:2357–2495
28. Wu SC (2000) Nuclear data sheets for A= 46. *Nucl Data Sheets* 91:1–116
29. Chen J (2022) Nuclear data sheets for A= 48. *Nucl Data Sheets* 179:1–382
30. Cameron J, Chen J, Singh B, Nica N (2012) Nuclear data sheets for A= 37. *Nucl Data Sheets* 113:365–514
31. Zs R, Firestone RB, Belgya T, Molnár, (2004) Prompt gamma-ray spectrum. In: Molnár GL (ed) *Handbook of prompt gamma activation analysis with neutron beams*. Kluwer Academic Publishers, Dordrecht/Boston/New York, pp 173–364
32. Barzilov A, Womble P (2014) Study of doppler broadening of gamma-ray spectra in 14-MeV neutron activation analysis. *J Radioanal Nucl Chem* 301:811–819
33. Catz AL, Amiel S (1967) Study of lifetimes of nuclear levels by doppler broadening attenuation using a (Ge)Li gamma-ray spectrometer. *Nucl Phys A* 92:222–232
34. Chu SYF, Ekström LP, Firestone RB (1999) WWW Table of Radioactive Isotopes, database Version 2.0 February 1999 <http://nucleardata.nuclear.lu.se/toi/index.asp>
35. OECD NEA Data Bank (2020) JANIS Book of neutron-induced cross-sections <https://www.oecd-nea.org/janis/book/book-neutron-2020-09.pdf>
36. Nuclear Data Center, (1996) Japan Atomic Energy Agency, Tables of Nuclear Data <https://www.ndc.jaea.go.jp/jendl/j40/j40.html>
37. Shibata K, Iwamoto O, Nakagawa T, Iwamoto N, Ichihara A, Kunieda S, Chiba S, Furutaka K, Otuka N, Ohsawa T, Murata T, Matsunobu H, Zukeran A, Kamada S, Katakura J (2010) JENDL-40: a new library for nuclear science and engineering. *J Nucl Sci Technol* 48(1):1–30
38. Brown DA et al (2018) ENDF/B-VIII.0: the 8th major release of the nuclear reaction data library with CIELO-project cross sections, new standards and thermal scattering data. *Nucl Data Sheets* 148:1–142
39. MacFarlane RE, Kahler AC (2010) Methods for processing ENDF/B-VII with NJOY. *Nucl Data Sheets* 111:2739–2890
40. MacFarlane R, Muir DW, Boicourt RM, Kahler AC, Conlin JL (2017) The NJOY nuclear data processing system. Version. <https://doi.org/10.2172/1338791>
41. Dickens JK (1972) The neutron induced gamma-ray reactions in calcium in the energy range  $4.85 \leq E_n \leq 8.05$  MeV. *Nucl Sci Eng* 48:78–86
42. Tellez A, Ronsin H, Ballini R, Fodor I (1973) Excited states of  $^{40}\text{Ca}$  up to 9 MeV. *J Phys (Paris)* 34:281–293
43. NIST XCOM: Photons Cross Sections Database, National Institute of Standards and Technology <https://physics.nist.gov/PhysRefData/Xcom/html/xcom1.html>
44. Zs R (2009) Determining elemental composition using prompt  $\gamma$  activation analysis. *Anal Chem.* <https://doi.org/10.1021/ac9011705>

**Publisher's Note** Springer Nature remains neutral with regard to jurisdictional claims in published maps and institutional affiliations.